PCCP

Molecular Simulation of Glycerol-Derived Triether Podands for Lithium Ion Solvation

Journal:	*Physical Chemistry Chemical Physics*
Manuscript ID	CP-ART-02-2022-000646.R2
Article Type:	Paper
Date Submitted by the Author:	24-Mar-2022
Complete List of Authors:	Barbosa, Gabriel; The University of Alabama, Chemical and Biological Engineering Bara, Jason; University of Alabama, Chemical & Biological Engineering; www.ua.edu Turner, Christoffer; The University of Alabama, Chemical and Biological Engineering

Molecular Simulation of Glycerol-Derived Triether Podands for Lithium Ion Solvation

Gabriel D. Barbosa, Jason E. Bara, C. Heath Turner†

Department of Chemical and Biological Engineering, The University of Alabama, Tuscaloosa, AL 35487, USA

ABSTRACT: Solvate ionic liquids (ILs) are promising candidates for several applications due to their stability, high coulombic efficiency, and low volatility. In this work, we investigate the solvation of lithium-bistriflimide by different glycerol-derived triether solvents, using molecular dynamics simulations. Very strong interactions between Li^+ and the solvent oxygen sites are found, leading to significant conformational changes in the solvent. By comparing the conformation of the neat solvents with their IL mixtures at different concentrations and temperatures, we find that the presence of Li^+ induces a distinct crown-like structure in the solvent molecules. The Li^+ cations and the surrounding solvent form a podand complex, which is stable even at elevated temperatures. These glycerol-derived solvents exhibit distinct interactions with Li^+ cations which may be exploited in electrolytic applications or lithium recovery processes.

†Corresponding Author:
E-mail: hturner@eng.ua.edu
Phone: +1 (205) 348-1733

INTRODUCTION

Acyclic ether-based solvents have a tendency to coordinate with positively charged atoms to form crown-like structures, known as podands. These unique molecular complexes may be useful in a number of different applications.[1–3] For example, podands formed by a mixture of organic solvents and lithium salts (i.e., solvate ionic liquids (ILs)) have proven to be promising electrolyte candidates,[4–10] reaction media for organic reactions,[11,12] and sizing agents for carbon fibers.[13] For instance, Ueno et al.[10] experimentally showed that different solvate ILs composed of glymes (triglyme and tetraglyme) and Li^+ salts (i.e., Li(glyme)X complexes) exhibit beneficial characteristics for battery electrolytes, such as high ionicity, high oxidative stability, and low volatility. Different Li(glyme) complexes in different Li^+ batteries were observed to demonstrate promising performance, but some unwanted side reactions of the solvate IL-based electrolytes were detected.[9,14] To mitigate these reactions, it has been shown that the addition of fluorinated groups can significantly enhance the stability of some solvate ILs.[15–18]

The search for stable solvate ILs has mainly been conducted using trial and error approaches, based almost exclusively on experimental efforts. Some simulations have been performed to provide theoretical guidance, but the simulations have primarily been limited to quantum chemical (QC) studies of a single solvent molecule coordinated to Li^+ salts.[19,20] Although these fundamental interactions are important to quantify, more molecular-level information is needed regarding the intermolecular coordination environment of the system in a bulk solution, including an analysis of the relevant sites involved in the cation-cation, cation-anion, cation/anion-solvent, and solvent-solvent interactions. This information is crucial for predicting general performance trends and guiding the development of new solvent compounds.

Well known for its versatility and low cost, glycerol (propane-1,2,3-triol) has been widely used in several commercial markets, such as pharmaceuticals, oil, and the food industry.[21,22] Glycerol is generated in large quantities as a by-product of biodiesel production, and the expansion of biodiesel production worldwide has contributed considerably to the decrease in glycerol prices (the value is so low that it is often treated as a waste).[21] Thus, there is an opportunity to convert this low-cost feedstock into a higher value solvent, due to its chemical versatility and wide availability.[23–25] Very recently, Qian et al.[26,27] used a combination of experiments and simulations to show that different glycerol-derived compounds (e.g., triethers) have promising performance for CO_2 absorption; other applications of glycerol-derived solvents have been previously proposed in the literature.[24,28,29] Despite the similarities in the chemical structure of glycerol derived triethers and glymes, to the best of our knowledge, there are no experimental or computational studies of the solvation of Li^+ cations by glycerol-derived triethers. There are several technologies that may benefit from these compounds, including applications in battery electrolyte solutions and lithium recovery.

In this work, we use molecular simulations to investigate the solvation behavior of Li^+ by three glycerol-derived triether solvents bearing one, two, or three trifluoromethyl ($-CF_3$) groups; namely, 6-((2,2,2-trifluoroethoxy)methyl)-2,5,8,11-tetraoxadodecane (CAS: 2756130-95-5) (TRF1), 13,13,13-trifluoro-6-((2,2,2-trifluoroethoxy)methyl-2,5,8,11-tetraoxatridecane (TRF2), and 1,1,1,14,14,14-hexafluoro-7-((2,2,2-trifluoroethoxy)methyl)-3,6,9,12-tetraoxatetradecane (TRF3). In order to obtain information about the structural properties and conformations of these solvents, we first simulate the homogeneous bulk solvents. Then, we evaluate the solvent structural change that are induced by Li^+ in the bulk mixtures of these solvents by adding $LiTf_2N$

at different concentrations and at different temperatures. We find that there are very distinct crown-like solvent structures formed around the Li^+ atoms, and these complexes ("podands") maintain their stability even at elevated temperatures.

SIMULATION METHODOLOGY

The molecular dynamics (MD) simulations are performed using Gromacs 2021.1[30]; the PACKMOL package[31] is used to build the initial configurations in the simulation boxes. The bonded and non-bonded interactions of TRF1, TRF2, and TRF3 (Figure 1) are modeled using the OPLS-AA force field;[32,33] the Lennard-Jones parameters of the Li^+ cation are taken from Jensen et al.,[34] and the TIP4P model[35] is used for the water interactions. The OPLS parameters of TRF1, TRF2, and TRF3 are obtained from LigParGen[36], and the Tf_2N^- force field parameters and charges are taken from Doherty et al.[37] The isolated molecular structures of TRF1, TRF2, and TRF3 are optimized using density functional theory at the B3LYP/6-31G+(d,p) level of theory, as implemented in Gaussian09;[38] based on the optimized structures, the atomic partial charges are estimated using the ChelpG method;[39] the optimized structures were then used to build the MD simulation boxes, as described above. The electrostatic surface maps of TRF1, TRF2, and TRF3 are presented in Figure S1. Consistent with the OPLS force field, geometric combination rules are used to model unlike pair interactions.

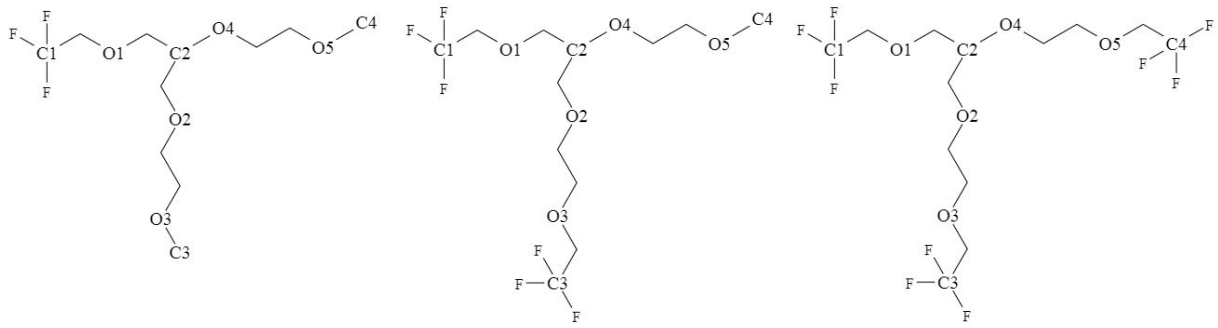

Figure 1. Molecular structure and atomic site labels of (a) TRF1, (b) TRF2, and TRF3.

The pure fluid thermodynamic and structural properties of the solvents are studied at 298, 323, and 348 K, using a system composed of 800 solvent (N_s=800) molecules. The mixtures of solvent + $LiTf_2N$ are composed of the same number of solvent molecules (N_s=800) and three different concentrations of $LiTf_2N$ (N_{LiTf2N} = 100, 200, and 300). The solvent-Li coordination is also evaluated in a bulk solvent + 1M $LiTf_2N$ brine mixture. The system compositions are summarized in Table 1.

The steepest descendent method is used to minimize the energy of the initial configurations, followed by a system equilibration stage of 350 ns in the isothermal-isobaric ensemble (NPT); an additional 50 ns of simulation in the NPT is used to evaluate thermodynamic and structural properties. The Parrinello-Rahman barostat[40,41] and the velocity rescaling thermostat[42] are used, with time constants of 0.1 and 5 ps, respectively. The leapfrog algorithm[43] is used to integrate the equations of motion using a time step of 2 fs, and periodic boundary conditions are applied in all directions. The hydrogen bonds are constrained using the LINCS algorithm, a cutoff distance of 1.2 nm is used for the Lennard-Jones and coulombic interactions, and the particle mesh Ewald (PME) method[44] is used to calculate the long-range electrostatic interactions. Figure 2 presents

snapshots of the final configurations of pure TRF1, TRF1+$LiTf_2N$, and 1M $LiTf_2N$ brine + TRF1, from which the increase in complexity of these systems can be explicitly observed.

Table 1. Summary of the system compositions.

System	Number of species present				
	TRF1	TRF2	TRF3	$LiTf_2N$	H_2O
Neat Solvent	800	-	-	-	-
	-	800	-	-	-
	-	-	800	-	-
$LiTf_2N$ + Solvent	800	-	-	100/200/300	
	-	800	-	100/200/300	-
	-	-	800	100/200/300	-
1 M $LiTf_2N$ Brine + Solvent	848	-	-	230	10,000
	-	687	-	230	10,000
	-	-	577	230	10,000

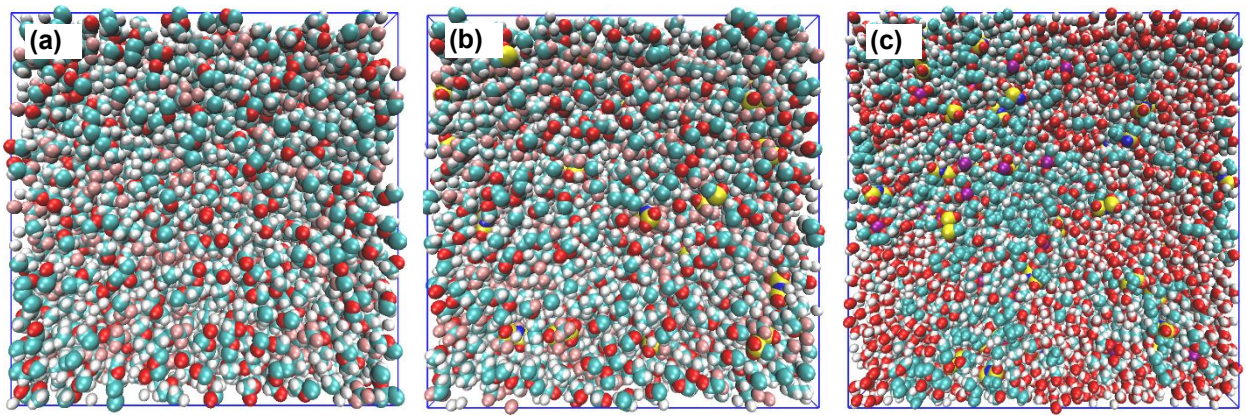

Figure 2. Representative snapshots of equilibrated systems: (a) bulk TRF1 (6.61×6.61×6.61 nm^3), (b) 100 $LiTf_2N$ + TRF1 (7.01×7.01×7.01 nm^3), and (c) 1M $LiTf_2N$ brine + TRF1 (8.79×8.79×8.79 nm^3) at 298 K and 1 bar. Color code: cyan = C, white = H, blue = nitrogen, red = O, yellow = S, pink = F.

RESULTS

Pure Bulk Solvent. The average mass densities and self-diffusion coefficients for the pure bulk solvents are summarized in Table 2. Although the densities of these solvents within this temperature range are generally similar, the average density increases from TRF1 to TRF3, as expected with increasing number of -CF_3 groups. Analogously, the self-diffusion coefficients follow the expected behavior with temperature, and they increase according to the trend TRF1 < TRF2 < TRF3.

Figure 3 shows the center-of-mass radial distribution functions (RDFs) of TRF1, TRF2 and TRF3 at 298 K. The RDFs are remarkably similar, with two main peaks; the first peak is around 0.55 nm, and the second centered around 1.2 nm; the first TRF3 peak is slightly less intense than the other solvents. The local coordination of neighboring O and F atoms around the studied solvent molecules can be explicitly observed by analyzing the spatial distribution functions shown in Figures S2 and S3. Notably, coordination of the C and O atoms around the branch point is observed; on the other hand, there is no preferential coordination of a specific site for the F atoms.

Table 2. Average density and self-diffusion coefficient of neat TRF1, TRF2, and TRF3 solvents at 298, 323, and 348 K and 1 bar.

System	Temperature (K)	Density (kg/m^3)	Diffusion (10^{-7} cm^2/s)
TRF1	298	1195.94	0.19
	323	1170.92	0.87
	348	1141.64	3.68
TRF2	298	1308.92	0.33
	323	1277.33	1.40
	348	1244.85	4.37

TRF3	298	1391.20	0.44
	323	1356.09	2.00
	348	1320.62	5.65

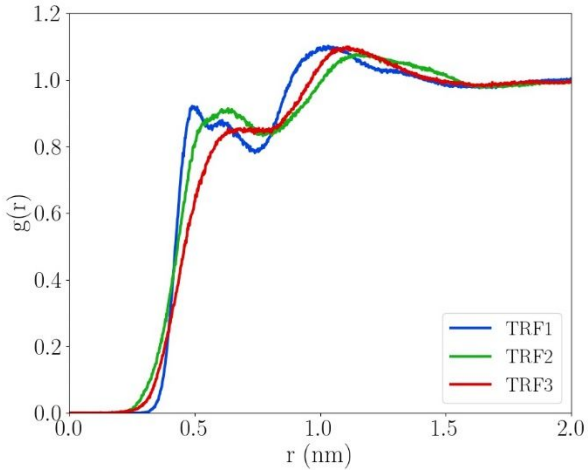

Figure 3. Solvent-solvent center-of-mass RDFs at 298 K and 1 bar for the neat solvent systems.

To characterize the average molecular structure of the solvents, the TRAVIS package[45,46] is used to obtain the combined distribution functions (CDFs) of the angles between the atoms C1-C2-C3 (θ) and C4-C2-C3 (φ). These angles can help characterize the relative structure (and deviations) among the three main segments of each solvent. The obtained CDFs for TRF1, TRF2, and TRF3 at 298 K are presented in Figure 4. For reference, it is worth noting that the default angles between the different branches extending from a central sp^3 carbon atom is approximately 109.5°.[47] The CDF for TRF1 shows a broad distribution, with a higher probability of θ ranging from 130° to 150° and φ ranging from 70° to 100°. Notably, very similar probability distributions are also observed for TRF2 and TRF3. However, these CDFs exhibit slightly polarized regions of φ, with bimodal peaks appearing around 45° and 90°.

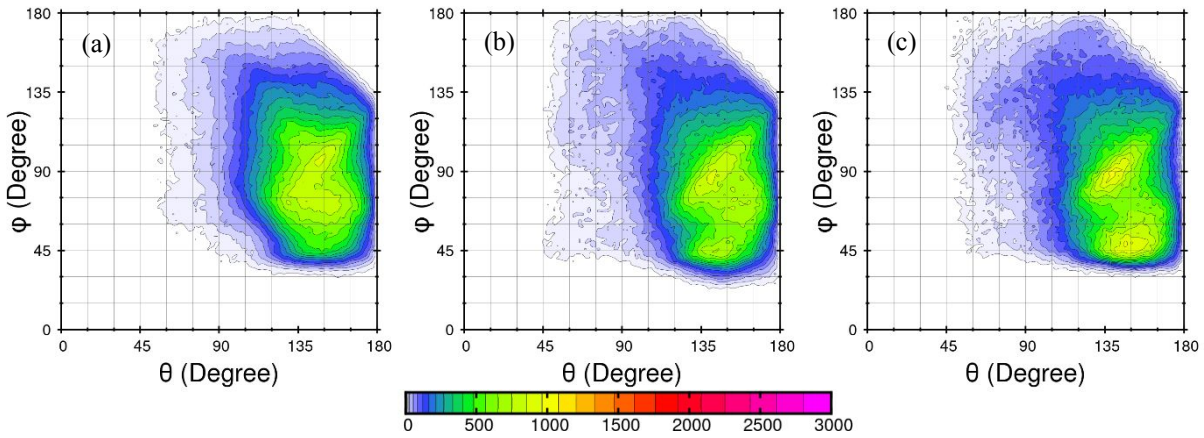

Figure 4. Neat solvent combined distribution functions of the angles C1-C2-C3 (θ) and C4-C2-C3 (φ) of (a) TRF1, (b) TRF2 and (c) TRF3 at 298 K and 1 bar. The color scale indicates the number of occurrences that fall within each angle bin.

Solvent + $LiTf_2N$ Mixtures. The RDFs for the bulk mixture of 100 $LiTf_2N$ + solvent at 298 K are shown in Figure 5, including the solvent-solvent center-of-mass, as well as the RDFs between Li^+ and ether -O- sites. As seen in Figure 5(a), TRF1-TRF1 exhibits a narrow first peak around 0.5 nm and a second broader one around 1.0~1.2 nm. Similar behavior is observed in the other RDFs presented in Figure 5(a). Nonetheless, the first peak is shifted to the right and is less intense for TRF2 and TRF3; the second peak is slightly shifted but not correlated to the structural trend of the solvents. Also, a small short-range peak is observed in the RDF of TRF3. When comparing Figure 5(a) with Figure 3, the presence of $LiTf_2N$ introduces a differentiating effect among the solvent-solvent coordination, which is associated with a configurational change of the solvent structure due to the presence of the Li^+ cation, as shown in more detail below. Regarding anion-cation coordination, Figure 5(b) shows that the Li^+-Tf_2N^- RDFs exhibit similar qualitative behavior for all solvents, characterized by the formation of two peaks centered around 0.5 nm, with the

second peak notably more intense than the first. The Li^+-Tf_2N^- second peak is remarkably more intense for TRF3 than the other solvents.

Based on Figure 5, there is strong coordination between the ether -O- sites of the solvents with Li^+, with the most intense and short-range interactions appearing at the O2 and O4 sites. Notably, strong coordination of Li^+-O2 is observed for TRF1 and TRF3; on the other hand, stronger Li^+-O4 coordination is observed for TRF2. When comparing the different solvents, it is observed that Li^+-O2 coordination is slightly more intense for TRF3. It is worth highlighting that the interaction between the O and Li^+ sites due to the presence of $-CF_3$ groups at the ends of the ether chains is in good agreement with the experimental results obtained previously by Yip et al.[4]; namely, the functionalization of the glycerol-based solvent by the electron-withdrawing $-CF_3$ group does not significantly impact the coordination between the O and Li^+ sites (only a small decrease is observed). By integrating the first peak of the RDFs between Li^+ and O2, we calculate average Li^+-O2 coordination numbers of 1.73 ± 0.08, 1.55 ± 0.06, and 1.54 ± 0.03 for TRF1, TRF2, and TRF3, respectively (95% confidence intervals are obtained by averaging the coordination numbers from three independent simulation trajectories).

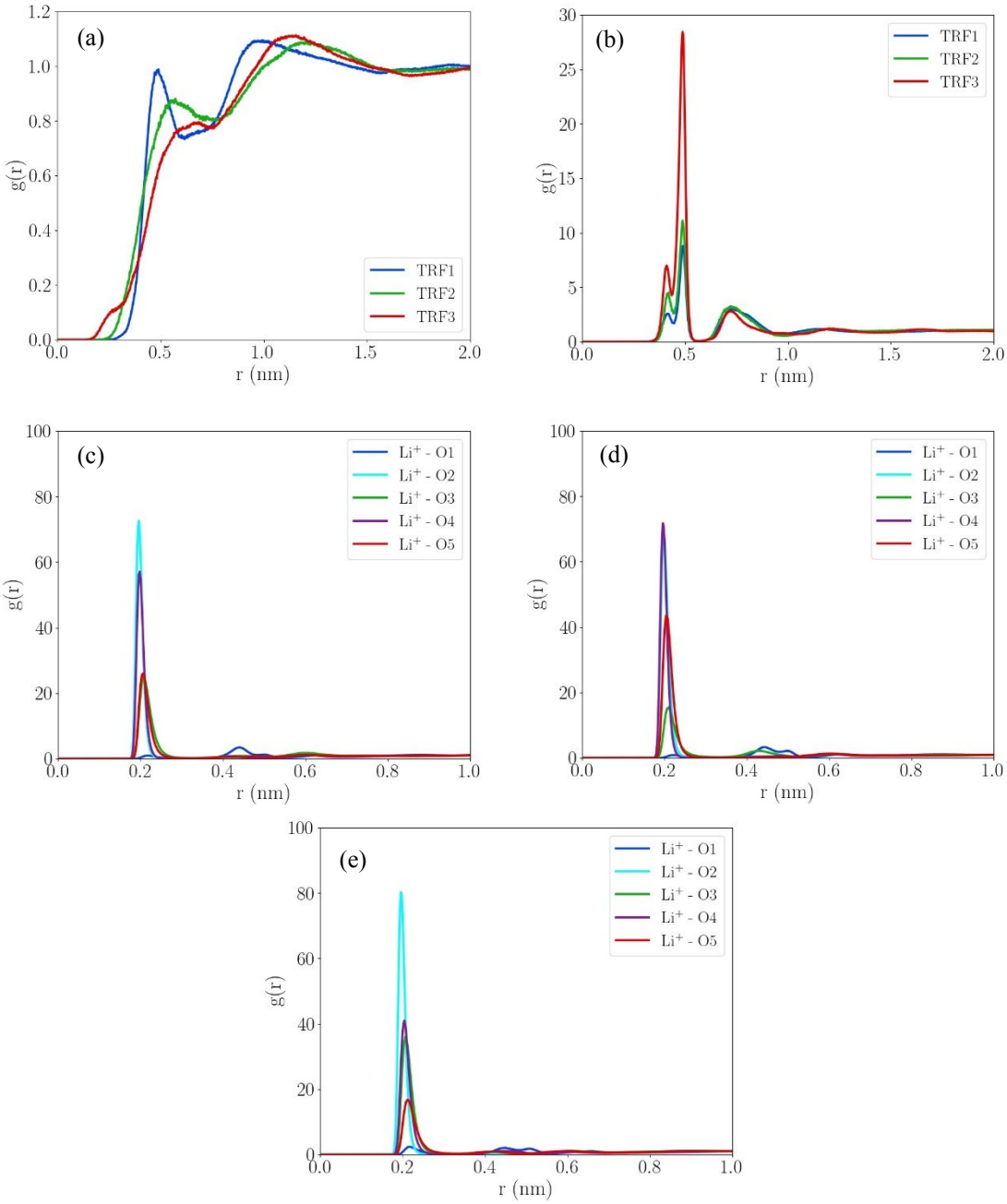

Figure 5. RDF plots for the mixture of 100 $LiTf_2N$ + solvent at 298 K: (a) solvent-solvent COM, (b) Li^+-Tf_2N^- COM, (c) Li^+ and O sites of TRF1, (d) Li^+ and O sites of TRF2, and (e) Li^+ and O sites of TRF3.

The effect of temperature on the site-site interactions is illustrated in Figures S4-S6. In all solvents, the increase in temperature leads to a slight increase in the coordination between the ether -O- sites and the Li^+ cation, suggesting more intense interaction at higher temperatures. The counterintuitive temperature sensitivity of the coordination between the oxygen and Li^+ sites has been previously observed for a similar tetraglyme solvent.[48] The RDFs between Li^+ and the oxygen sites shown in Figure 5 have also been numerically evaluated (Table S1), by identifying the most intense peak position, its intensity, potential of mean force (assessed using the RDF at the most intense peak position), and coordination number up to 0.4 nm. Although stronger Li^+-O2 coordination is observed for TRF3 at 298 K, the coordination sensitivity between Li^+ sites and oxygen is notably lower for TRF3 than for the other solvents. The podand configuration is primarily involved with the oxygen sites located at O2-O5. The total Li^+ coordination from these four oxygen sites decreases slightly as the amount of fluorination increases, with corresponding values at 298 K/348 K shown in parentheses: TRF1 (5.5/6.3); TRF2 (5.3/6.1); TRF3 (4.9/5.1). Table S2 presents the partial charges of the oxygen sites of the solvents analyzed here, obtained using the ChelpG method. As observed, the oxygen sites O2-O5 have higher electronegative charges, suggesting that the Li^+ coordination by these sites is due to stronger Li^+-O electrostatic interactions.

Similar to the pure bulk solvents, we also evaluate the solvent molecular conformations in the mixtures with $LiTf_2N$ by calculating the CDFs of the θ and φ angles. The CDF results for the solvent mixture with 100 $LiTf_2N$ molecules at 298 K are presented in Figure 6. In general, the populated regions of the CDFs are remarkably similar to the distributions presented in Figure 4. There is a narrow distribution of θ ranging from 130° to 180°, but on the other hand, there is a

broader distribution of φ, from 45° up to around 120°. However, despite these similarities, the CDFs presented in Figure 6 show more defined distributions, in which the most probable values of θ and φ are situated around 45° and 140°, respectively. The influence of $LiTf_2N$ concentration on the CDFs of these angles can be seen in Figures S7-S9, in which the most likely values of θ and φ remain consistent (around 45° and 140° for θ and φ, respectively); interestingly, the peak probability distributions become significantly enhanced with increasing $LiTf_2N$ concentration.

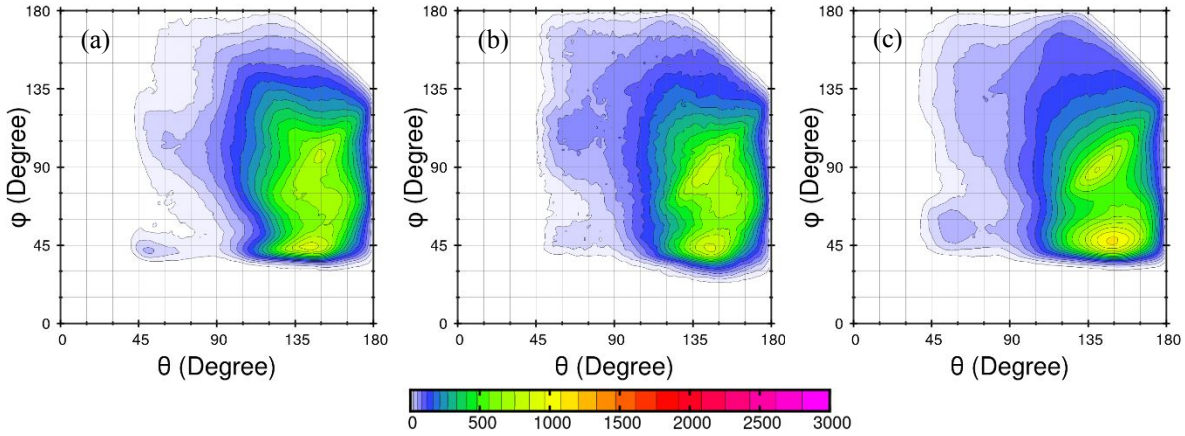

Figure 6. Combined distribution functions of the θ and φ angles for the mixture of 100 $LiTf_2N$ + solvent at 298 K: (a) TRF1, (b) TRF2, and (c) TRF3. The color scale indicates the number of occurrences that fall within each angle bin.

Overall, based on these CDFs and the RDFs presented earlier, we conclude that the presence of Li^+ induces a crown-like structure in the studied solvents, in which Li^+ is solvated by a highly-structured solvent backbone motif involving the O2-O5 oxygen sites. This solvation behavior can be explicitly observed by examining the spatial distribution functions displayed in Figure 7. This distinct solvation structure has also been observed before for different ether-based solvents, based mainly on Raman spectroscopic analysis, and QC calculations.[4,48–52] Due to the high computational

cost, the quantum chemical studies are very limited in size (e.g., only one solvent molecule and a few ions present in the calculation). The results obtained here are designed to emulate conditions that are much more representative of the bulk solution environment. Overall, we find that even with competing interactions present in the bulk solvent and the addition of thermal motions, the Li^+ podand motif remains very strong.

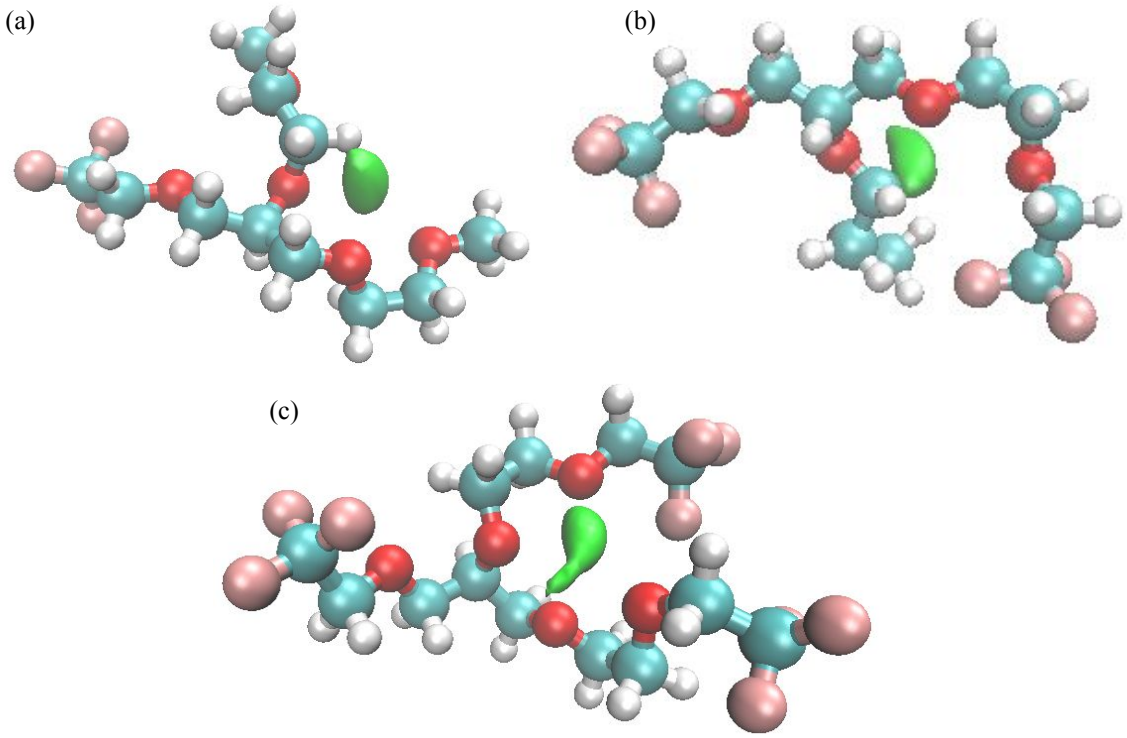

Figure 7. Spatial distribution function of Li^+ (green isosurface) around (a) TRF1, (b) TRF2, and (c) TRF3 for the mixture of 200 $LiTf_2N$ + solvent at 298 K and 1 bar. Color code: cyan = carbon; white = hydrogen; pink = fluorine.

Finally, we investigate the coordination between Li^+ and the oxygen sites of TRF1, TRF2, and TRF3 in a bulk mixture of these solvents with a 1M brine solution of $LiTf_2N$. Figure S10 shows the corresponding RDFs. The coordination between the Li^+ and ether -O- sites is very similar to

the behavior of the previous mixtures studied (i.e., Fig. 5). There is strong Li^+-O2 coordination for TRF1 and TRF3, and strong coordination of Li^+ by the O4 site of TRF2. In addition, the conformation of the solvent molecules in crown-like podand structures can be detected by looking at the CDFs shown in Figure S11.

CONCLUSIONS

In this work, we use MD simulations to investigate the molecular structure and solvation behavior of $LiTf_2N$ in three glycerol-derived triether solvents. Based on RDF analyses, we find strong interactions between Li^+ and the solvent oxygen sites. Consistent with other literature reports, the fluorination of the solvent does not significantly change the Li^+-O interactions in our systems. Furthermore, we find that increasing the temperature from 298 to 348 K slightly enhances this coordination, although the fully fluorinated solvent demonstrates negligible temperature sensitivity. A comprehensive analysis of the solvent structures using CDFs together with the RDFs at different $LiTf_2N$ concentrations indicates the formation of distinct crown-like structures (podands), in which the solvent chains enclose the Li^+ cations. The results obtained here highlight the distinct interactions between three different glycerol-derived solvents with Li^+ ions, and this may benefit the development of new electrolyte compositions or solvents for Li^+ recovery.

Declaration of Competing Interest

The authors declare that they have no known competing financial interests or personal relationships that could have appeared to influence the work reported in this paper.

Acknowledgements

This work is supported by the Alabama Advanced Solvent Cluster (AASC), funded by the U.S. Department of Energy Established Program to Stimulate Competitive Research (DOE-EPSCoR) (DE-SC0020282). We are grateful to the Alabama Supercomputer Authority for computational support and for a UA CyberSeed grant.

Supporting Information Available: This material is available free of charge via the Internet. Electrostatic surface potentials of the solvents; spatial distribution functions of the solvents; additional RDF plots and quantitative analyses of coordination; additional CDFs of the solvents.

References

(1) Weber, E.; Vögtle, F. Classification and Nomenclature of Coronands, Cryptands, Podands, and of Their Complexes. *Inorganica Chim. Acta* **1980**, *45*, L65–L67. https://doi.org/10.1016/S0020-1693(00)80096-1.

(2) Vögtle, F.; Weber, E. Multidentate Acyclic Neutral Ligands and Their Complexation. *Angew. Chemie Int. Ed. English* **1979**, *18* (10), 753–776. https://doi.org/10.1002/anie.197907531.

(3) Filatova, E. S.; Fedorova, O. V.; Rusinov, G. L.; Charushin, V. N. Synthesis and Properties of Heterocycle-Containing Podands. *Chem. Heterocycl. Compd.* **2021**, *57* (10), 971–983. https://doi.org/10.1007/s10593-021-03009-y.

(4) Yu, Z.; Wang, H.; Kong, X.; Huang, W. W. W.; Tsao, Y.; Mackanic, D. G.; Wang, K.; Wang, X.; Huang, W. W. W.; Choudhury, S.; Zheng, Y.; Amanchukwu, C. V.; Hung, S. T.; Ma, Y.; Lomeli, E. G.; Qin, J.; Cui, Y.; Bao, Z. Molecular Design for Electrolyte Solvents Enabling Energy-Dense and Long-Cycling Lithium Metal Batteries. *Nat. Energy* **2020**, *5* (7), 526–533. https://doi.org/10.1038/s41560-020-0634-5.

(5) Marangon, V.; Hernandez-Rentero, C.; Levchenko, S.; Bianchini, G.; Spagnolo, D.; Caballero, A.; Morales, J.; Hassoun, J. Lithium–Oxygen Battery Exploiting Highly Concentrated Glyme-Based Electrolytes. *ACS Appl. Energy Mater.* **2020**, *3* (12), 12263–12275. https://doi.org/10.1021/acsaem.0c02331.

(6) Mandai, T.; Dokko, K.; Watanabe, M. Solvate Ionic Liquids for Li, Na, K, and Mg

Batteries. *Chem. Rec.* **2019**, *19* (4), 708–722. https://doi.org/10.1002/tcr.201800111.

(7) Krampa, F.; Aniweh, Y.; Awandare, G.; Kanyong, P. A Disposable Amperometric Sensor Based on High-Performance PEDOT:PSS/Ionic Liquid Nanocomposite Thin Film-Modified Screen-Printed Electrode for the Analysis of Catechol in Natural Water Samples. *Sensors* **2017**, *17* (8), 1716. https://doi.org/10.3390/s17081716.

(8) Nakazawa, T.; Ikoma, A.; Kido, R.; Ueno, K.; Dokko, K.; Watanabe, M. Effects of Compatibility of Polymer Binders with Solvate Ionic Liquid Electrolytes on Discharge and Charge Reactions of Lithium-Sulfur Batteries. *J. Power Sources* **2016**, *307*, 746–752. https://doi.org/10.1016/j.jpowsour.2016.01.045.

(9) Ueno, K.; Park, J.-W.; Yamazaki, A.; Mandai, T.; Tachikawa, N.; Dokko, K.; Watanabe, M. Anionic Effects on Solvate Ionic Liquid Electrolytes in Rechargeable Lithium–Sulfur Batteries. *J. Phys. Chem. C* **2013**, *117* (40), 20509–20516. https://doi.org/10.1021/jp407158y.

(10) Ueno, K.; Yoshida, K.; Tsuchiya, M.; Tachikawa, N.; Dokko, K.; Watanabe, M. Glyme–Lithium Salt Equimolar Molten Mixtures: Concentrated Solutions or Solvate Ionic Liquids? *J. Phys. Chem. B* **2012**, *116* (36), 11323–11331. https://doi.org/10.1021/jp307378j.

(11) Eyckens, D. J.; Henderson, L. C. Synthesis of α-Aminophosphonates Using Solvate Ionic Liquids. *RSC Adv.* **2017**, *7* (45), 27900–27904. https://doi.org/10.1039/C7RA04407K.

(12) Schaffarczyk McHale, K. S.; Wong, M. J.; Evans, A. K.; Gilbert, A.; Haines, R. S.; Harper, J. B. Understanding the Effects of Solvate Ionic Liquids as Solvents on Substitution Processes. *Org. Biomol. Chem.* **2019**, *17* (41), 9243–9250. https://doi.org/10.1039/C9OB01753D.

(13) Eyckens, D. J.; Servinis, L.; Scheffler, C.; Wölfel, E.; Demir, B.; Walsh, T. R.; Henderson, L. C. Synergistic Interfacial Effects of Ionic Liquids as Sizing Agents and Surface Modified Carbon Fibers. *J. Mater. Chem. A* **2018**, *6* (10), 4504–4514. https://doi.org/10.1039/C7TA10516A.

(14) Kwon, H.-M.; Thomas, M. L.; Tatara, R.; Oda, Y.; Kobayashi, Y.; Nakanishi, A.; Ueno, K.; Dokko, K.; Watanabe, M. Stability of Glyme Solvate Ionic Liquid as an Electrolyte for Rechargeable Li−O 2 Batteries. *ACS Appl. Mater. Interfaces* **2017**, *9* (7), 6014–6021. https://doi.org/10.1021/acsami.6b14449.

(15) Li, T.; Zhang, X.-Q.; Shi, P.; Zhang, Q. Fluorinated Solid-Electrolyte Interphase in High-Voltage Lithium Metal Batteries. *Joule* **2019**, *3* (11), 2647–2661. https://doi.org/10.1016/j.joule.2019.09.022.

(16) Jiao, S.; Ren, X.; Cao, R.; Engelhard, M. H.; Liu, Y.; Hu, D.; Mei, D.; Zheng, J.; Zhao,

W.; Li, Q.; Liu, N.; Adams, B. D.; Ma, C.; Liu, J.; Zhang, J.-G.; Xu, W. Stable Cycling of High-Voltage Lithium Metal Batteries in Ether Electrolytes. *Nat. Energy* **2018**, *3* (9), 739–746. https://doi.org/10.1038/s41560-018-0199-8.

(17) Qian, J.; Henderson, W. A.; Xu, W.; Bhattacharya, P.; Engelhard, M.; Borodin, O.; Zhang, J.-G. High Rate and Stable Cycling of Lithium Metal Anode. *Nat. Commun.* **2015**, *6* (1), 6362. https://doi.org/10.1038/ncomms7362.

(18) Aurbach, D.; Granot, E. The Study of Electrolyte Solutions Based on Solvents from the "Glyme" Family (Linear Polyethers) for Secondary Li Battery Systems. *Electrochim. Acta* **1997**, *42* (4), 697–718. https://doi.org/10.1016/S0013-4686(96)00231-9.

(19) Chen, X.; Yao, N.; Zeng, B.-S.; Zhang, Q. Ion–Solvent Chemistry in Lithium Battery Electrolytes: From Mono-Solvent to Multi-Solvent Complexes. *Fundam. Res.* **2021**, *1* (4), 393–398. https://doi.org/10.1016/j.fmre.2021.06.011.

(20) Chen, X.; Zhang, Q. Atomic Insights into the Fundamental Interactions in Lithium Battery Electrolytes. *Acc. Chem. Res.* **2020**, *53* (9), 1992–2002. https://doi.org/10.1021/acs.accounts.0c00412.

(21) Bagnato, G.; Iulianelli, A.; Sanna, A.; Basile, A. Glycerol Production and Transformation: A Critical Review with Particular Emphasis on Glycerol Reforming Reaction for Producing Hydrogen in Conventional and Membrane Reactors. *Membranes (Basel).* **2017**, *7* (2), 17. https://doi.org/10.3390/membranes7020017.

(22) Tan, H. W.; Abdul Aziz, A. R.; Aroua, M. K. Glycerol Production and Its Applications as a Raw Material: A Review. *Renew. Sustain. Energy Rev.* **2013**, *27*, 118–127. https://doi.org/10.1016/j.rser.2013.06.035.

(23) Andreeva, I. V.; Zaitsau, D. H.; Qian, S.; Turovtzev, V. V.; Pimerzin, A. A.; Bara, J. E.; Verevkin, S. P. Glycerol Valorisation towards Biofuel Additivities: Thermodynamic Studies of Glycerol Ethers. *Chem. Eng. Sci.* **2022**, *247*, 117032. https://doi.org/10.1016/j.ces.2021.117032.

(24) García, J. I.; García-Marín, H.; Mayoral, J. A.; Pérez, P. Quantitative Structure–Property Relationships Prediction of Some Physico-Chemical Properties of Glycerol Based Solvents. *Green Chem.* **2013**, *15* (8), 2283. https://doi.org/10.1039/c3gc40694f.

(25) García, J. I.; García-Marín, H.; Mayoral, J. A.; Pérez, P. Green Solvents from Glycerol. Synthesis and Physico-Chemical Properties of Alkyl Glycerol Ethers. *Green Chem.* **2010**, *12* (3), 426. https://doi.org/10.1039/b923631g.

(26) Qian, S.; Liu, X.; Turner, C. H.; Bara, J. E. Synthesis and Properties of Symmetric Glycerol-Derived 1,2,3-Triethers and 1,3-Diether-2-Ketones for CO2 Absorption. *Chem. Eng. Sci.* **2022**, *248*, 117150. https://doi.org/10.1016/j.ces.2021.117150.

(27) Qian, S.; Liu, X.; Turner, C. H.; Bara, J. E. Glycerol-derived Solvents Containing Two or Three Distinct Functional Groups Enabled by Trifluoroethyl Glycidyl Ether. *AIChE J.* **2021**. https://doi.org/10.1002/aic.17533.

(28) Ampatzidis, C. D.; Varka, E.-M. A.; Karapantsios, T. D. Interfacial Activity of Amino Acid-Based Glycerol Ether Surfactants and Their Performance in Stabilizing O/W Cosmetic Emulsions. *Colloids Surfaces A Physicochem. Eng. Asp.* **2014**, *460*, 176–183. https://doi.org/10.1016/j.colsurfa.2014.02.033.

(29) Zaffalon, P.-L.; Zumbuehl, A. BODP - A Versatile Reagent for Phospholipid Synthesis. *Synthesis (Stuttg).* **2011**, *2011* (05), 778–782. https://doi.org/10.1055/s-0030-1258427.

(30) Lindahl; Abraham; Hess; Spoel, van der. GROMACS 2021.1 Source Code. **2021**. https://doi.org/10.5281/ZENODO.4561626.

(31) Martinez, L.; Andrade, R.; Birgin, E. G.; Martinez, J. M. PACKMOL: A Package for Building Initial Configurations for Molecular Dynamics Simulations. *J. Comput. Chem.* **2009**, *30* (13), 2157–2164.

(32) Jorgensen, W. L.; Maxwell, D. S.; Tirado-Rives, J. Development and Testing of the OPLS All-Atom Force Field on Conformational Energetics and Properties of Organic Liquids. *J. Am. Chem. Soc.* **1996**, *118* (45), 11225–11236.

(33) Jorgensen, W. L.; Tirado-Rives, J. The {OPLS} Force Field for Proteins. Energy Minimizations for Crystals of Cyclic Peptides and Crambin. *J. Am. Chem. Soc.* **1988**, *110* (6), 1657–1666.

(34) Jensen, K. P.; Jorgensen, W. L. Halide, Ammonium, and Alkali Metal Ion Parameters for Modeling Aqueous Solutions. *J. Chem. Theory Comput.* **2006**, *2* (6), 1499–1509. https://doi.org/10.1021/ct600252r.

(35) Jorgensen, W. L.; Chandrasekhar, J.; Madura, J. D.; Impey, R. W.; Klein, M. L. Comparison of Simple Potential Functions for Simulating Liquid Water. *J. Chem. Phys.* **1983**, *79* (2), 926–935. https://doi.org/10.1063/1.445869.

(36) Dodda, L. S.; de Vaca, I.; Tirado-Rives, J.; Jorgensen, W. L. LigParGen Web Server: An Automatic OPLS-AA Parameter Generator for Organic Ligands. *Nucleic Acids Res.* **2017**, *45* (W1), W331--W336.

(37) Doherty, B.; Zhong, X.; Gathiaka, S.; Li, B.; Acevedo, O. Revisiting OPLS Force Field Parameters for Ionic Liquid Simulations. *J. Chem. Theory Comput.* **2017**, *13* (12), 6131–6145. https://doi.org/10.1021/acs.jctc.7b00520.

(38) Frisch, M. J.; Trucks, G. W.; Schlegel, H. B.; Scuseria, G. E.; Cheeseman, J. R.; Scalmani, G.; Barone, V.; Mennucci, B.; Petersson, G. A. Gaussian 09. *Gaussian Inc. Wallingford*

CT 2009.

(39) Breneman, C. M.; Wiberg, K. B. Determining Atom-Centered Monopoles from Molecular Electrostatic Potentials. The Need for High Sampling Density in Formamide Conformational Analysis. *J. Comput. Chem.* **1990**, *11* (3), 361–373. https://doi.org/10.1002/jcc.540110311.

(40) Nosé, S.; Klein, M. L. Constant Pressure Molecular Dynamics for Molecular Systems. *Mol. Phys.* **1983**, *50* (5), 1055–1076.

(41) Parrinello, M.; Rahman, A. Polymorphic Transitions in Single Crystals: A New Molecular Dynamics Method. *J. Appl. Phys.* **1981**, *52* (12), 7182–7190.

(42) Bussi, G.; Donadio, D.; Parrinello, M. Canonical Sampling through Velocity Rescaling. *J. Chem. Phys.* **2007**, *126* (1), 14101.

(43) Hockney, R. .; Goel, S. .; Eastwood, J. . Quiet High-Resolution Computer Models of a Plasma. *J. Comput. Phys.* **1974**, *14* (2), 148–158. https://doi.org/10.1016/0021-9991(74)90010-2.

(44) Darden, T.; York, D.; Pedersen, L. Particle Mesh Ewald: An Nlog (N) Method for Ewald Sums in Large Systems. *J. Chem. Phys.* **1993**, *98* (12), 10089–10092.

(45) Brehm, M.; Thomas, M.; Gehrke, S.; Kirchner, B. TRAVIS—A Free Analyzer for Trajectories from Molecular Simulation. *J. Chem. Phys.* **2020**, *152* (16), 164105. https://doi.org/10.1063/5.0005078.

(46) Brehm, M.; Kirchner, B. TRAVIS - A Free Analyzer and Visualizer for Monte Carlo and Molecular Dynamics Trajectories. *J. Chem. Inf. Model.* **2011**, *51* (8), 2007–2023. https://doi.org/10.1021/ci200217w.

(47) Rowell, J. C.; Phillips, W. D.; Melby, L. R.; Panar, M. NMR Studies of Some Liquid Crystal Systems. *J. Chem. Phys.* **1965**, *43* (10), 3442–3454. https://doi.org/10.1063/1.1696498.

(48) Dong, D.; Bedrov, D. Charge Transport in [Li(Tetraglyme)][Bis(Trifluoromethane) Sulfonimide] Solvate Ionic Liquids: Insight from Molecular Dynamics Simulations. *J. Phys. Chem. B* **2018**, *122* (43), 9994–10004. https://doi.org/10.1021/acs.jpcb.8b06913.

(49) Callsen, M.; Sodeyama, K.; Futera, Z.; Tateyama, Y.; Hamada, I. The Solvation Structure of Lithium Ions in an Ether Based Electrolyte Solution from First-Principles Molecular Dynamics. *J. Phys. Chem. B* **2017**, *121* (1), 180–188. https://doi.org/10.1021/acs.jpcb.6b09203.

(50) Tsuzuki, S.; Shinoda, W.; Matsugami, M.; Umebayashi, Y.; Ueno, K.; Mandai, T.; Seki,

S.; Dokko, K.; Watanabe, M. Structures of [Li(Glyme)] + Complexes and Their Interactions with Anions in Equimolar Mixtures of Glymes and Li[TFSA]: Analysis by Molecular Dynamics Simulations. *Phys. Chem. Chem. Phys.* **2015**, *17* (1), 126–129. https://doi.org/10.1039/C4CP04718D.

(51) Mandai, T.; Yoshida, K.; Tsuzuki, S.; Nozawa, R.; Masu, H.; Ueno, K.; Dokko, K.; Watanabe, M. Effect of Ionic Size on Solvate Stability of Glyme-Based Solvate Ionic Liquids. *J. Phys. Chem. B* **2015**, *119* (4), 1523–1534. https://doi.org/10.1021/jp508100s.

(52) Ueno, K.; Tatara, R.; Tsuzuki, S.; Saito, S.; Doi, H.; Yoshida, K.; Mandai, T.; Matsugami, M.; Umebayashi, Y.; Dokko, K.; Watanabe, M. Li + Solvation in Glyme–Li Salt Solvate Ionic Liquids. *Phys. Chem. Chem. Phys.* **2015**, *17* (12), 8248–8257. https://doi.org/10.1039/C4CP05943C.